**Proceedings of ASME Turbo Expo 2017: Turbomachinery Technical Conference and Exposition**
**GT2017**
**June 26-30, 2017, Charlotte, NC USA**

# GT2017-64693

## A coupled 1D film hydrodynamics and core gas flow model for air-oil flows in aero-engine bearing chambers

**B. Kakimpa, H.P. Morvan and S. Hibberd**
Gas Turbine and Transmissions Research Centre (G2TRC),
The University of Nottingham, Nottingham, NG7 2RD, UK

### Abstract
*A robust 1D film hydrodynamic model has been sequentially coupled with a 1D core gas model and used to predict the instantaneous mean core gas speed, film interface shear stress and liquid film distribution within an idealised bearing chamber. This novel approach to aero-engine bearing chamber simulation provides a predictive tool that can be used for the fast and reliable exploration of a set of bearing chamber design and operating conditions characterised by the: chamber dimensions, air/oil fluid properties, shaft speed, sealing air flows, oil feed rates and sump scavenge ratios. A preliminary validation of the model against available bearing chamber flow measurements from literature shows good agreement. The model represents a significant step change in predictive capabilities for aero-engine oil system flows compared to previous semi-empirical models. The bearing chamber is idealised as a one-dimensional (2D) domain with a predominantly azimuthal flow in both the rotational oil film and core gas such that axial components may be ignored. A 1D system of depth-averaged film hydrodynamics equations is used to predict oil film thickness and mean speed distributions in the azimuthal direction under the influence of interface shear, gravity, pressure gradient and surface tension forces. The driving shear stress in the film model is obtained from the 1D core-gas model based on an azimuthal gas momentum conservation equation which is coupled to the film model through the interface shear stress and film interface velocity.*

### 1. Introduction
As a result of the interactions between the oil supply, the rotating core air flow and the sealing air inflow, complex multiphase flow patterns may be observed within the chamber. These flow regimes have been characterised by a number of experimental studies [1, 2, 3] and CFD simulations [4, 5] of bearing chambers. Figure 1 illustrates the flow within a typical aero-engine bearing chamber flow.

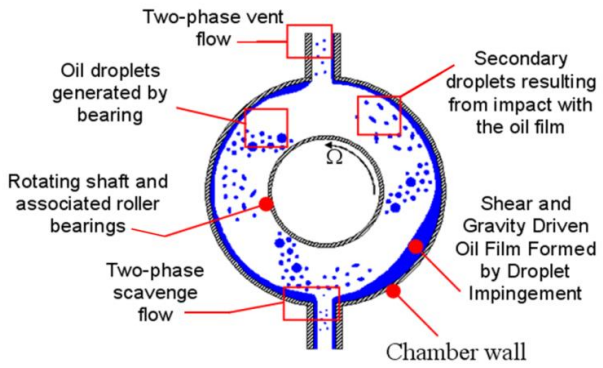


Figure 1: Schematic of a typical aero-engine bearing chamber operation [6]

The successful operation of aero-engine transmissions components requires the supply and efficient distribution of sufficient oil to lubricate and cool components such as bearings, gears and their surroundings. The oil supplied for this purpose is contained in air-sealed enclosures around the lubricated component to prevent leakages into the rest of the engine. The study of the oil regimes within these chambers and their dependence on the driving shear stress from the core air flow has been characterised by [1, 7, 8]. The design of these aero-engine bearing chambers required sufficient knowledge of the oil flow regime within the chamber to allow the delivery of sufficient cooling and lubrication while minimising power losses and oil degradation. The chamber design also needs to ensure that once the oil has achieved its intended purpose, it is efficiently scavenged from these chambers.

Experimental rigs such as in [1, 2, 3] may be used to iteratively test design performance however many of these rigs do not allow for a more detailed optimisation of design or give adequate

information on oil morphology and thermal map within the chamber at operating conditions to allow engineers to determine how best to improve the designs. In addition, this empirical data is often unavailable in the preliminary design stages. Recently, computational fluid dynamics has emerged as a valuable tool for obtaining more detailed insight into bearing chamber oil flow regimes as well as evaluating different design options in the early stages of design [5, 4, 6]. The main drawbacks of conventional CFD modelling is that it can be computationally expensive and hence unsuitable for the early stages of design during chamber sizing studies. There is a need to provide a reliable alternative in the form of a semi-analytical predictive tool for engineers to use in parametric studies aimed at the rapid assessment of chamber designs in the preliminary stages of design. This paper builds on previous research into film hydrodynamics [7, 8] and core gas dynamics modelling [9] to presents a novel modelling approach that is intended for this application.

Previously, Gorse et al [9] proposed a semi-empirical model for predicting core gas flow and the resulting oil film distribution within an aero-engine bearing chamber. The present model builds upon this work by providing further closure and removing some assumptions. While in the Gorse model [9] core gas flow and driving shear stress assumed a dry chamber condition, in the present study a new model for the non-uniform interfacial shear stress is introduced and coupled to the core gas and film hydrodynamics models. This approach takes into account the non-linear interaction between the air and the oil film which if present modifies gas dynamics by lowering resistance to flow.

In addition, the model presented in [9] assumed a simple shear-gravity balance within the film while the present study extends this work by including the effects of film inertia and other forces such as surface tension and pressure gradients which have been shown in [7] to play a vital role in pooling and shock type flow regimes that occur at lower shaft speeds. This extends the applicable range of the model from only high shear smooth flow regimes to low shear pooling and shock flow regimes where film backflows are known to occur and [9] demonstrated notable difficulties in obtaining solutions. Higher quartic film velocity profiles are also introduced in the inertia treatment of the present study to ensure that the effects of film re-circulations due to wall shear stress reversal are accurately accounted for.

Finally, while the Gorse model [9] is semi-empirical in nature, requiring a-priori knowledge of film thickness and velocity profile at a specified angular location, the present model introduces a predictive film hydrodynamics model which is coupled to a predictive code gas model. This makes the model suitable for predictive modelling applications such as in preliminary design assessment where empirical measurements of film thickness may not be available. This predictive model therefore represents a significant improvement to the current stare-of-the-art, relying only on design inputs such as the sealing air flow rate, shaft speed, oil feed rate, sump scavenge ratios and shaft/chamber geometry to obtain an estimate for both the core gas speed and film thickness and speed distribution.

The model is described in Section 2 and in Section 3 it is applied to the prediction of film thickness and speed distributions within a bearing chamber. Comparisons are made against experimental measurements and predictions from the Gorse model [9].

## 2. Coupled core gas and film model

The model is composed of two components; a 1D transient oil film hydrodynamics model after [7] which is used to predict oil film distribution and is described in section 2.1; a 1D core gas model after the work of [9] to predict the core gas speed within the chamber.

In the solution algorithm, this film hydrodynamics model is sequentially coupled with the core gas dynamics model via the interfacial shear stress from the air that is driving the film as well the film interface speed which is used in the core gas momentum balance equation. Both models use an explicit time-stepping routine and low courant numbers are required in order to guarantee numerical stability of the solution. The model was developed using a fourth order finite difference method for spatial discretisation and a first order explicit time scheme for temporal discretisation.

### 2.1. Oil film hydrodynamics model

The depth-averaged Eulerian thin-film modelling (ETFM) approach previously presented in [7] is used. In the ETFM model, the thin-film flow is idealised as a two-dimensional incompressible Newtonian liquid of density, $\rho_l$ and viscosity, $\mu_l$ flowing over a solid substrate and with a free-surface exposed to an incompressible Newtonian gas of density, $\rho_g$ and viscosity, $\mu_g$. The film has a spatially varying height, $h(s, t)$ and flows with a film velocity $u(s, y, t)$ - where $s$ is the horizontal flow direction and $y$ is the normal direction as shown in Figure 2. The setup shown in Figure 2 effectively corresponds to an incompressible, isothermal, gravity-shear driven rimming flow similar to that investigated by Kay et al. [8]. The resulting film flow dynamics over the solid-substrate may be described by the depth averaged continuity and momentum equations given by Equations (1) and (2).

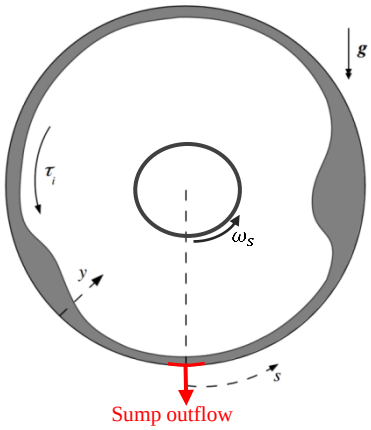


Figure 2 Thin-film rimming flow geometry and coordinate reference system used in the ETFM approach

$$\frac{\partial h}{\partial t}+\frac{\partial q}{\partial s}=S_m, \tag{1}$$

$$\frac{\partial q}{\partial t}+\frac{\partial}{\partial s}\int_0^h uudy = -\frac{h}{\rho_l}\frac{\partial p_l}{\partial s}+\frac{h}{\rho_l}\frac{\partial \sigma\kappa}{\partial s}+g_y h+S_\tau + S_{MOM}. \tag{2}$$

Where $p_l = (p_g - \rho g_y h)$, is the film pressure which has a component from the interfacial gas pressure, $p_g$, and the film hydrostatic pressure, $\rho g_y h$. $p_l$ is used to compute the film hydrostatic pressure gradient term, which is the first term on the right hand side (R.H.S.) of Equations (2). $S_m$ and $S_{MOM}$ are generic mass and source terms for the film domain.

Surface tension effects are represented in the surface tension term (second term on the R.H.S. of Equation (2)), where σ is the surface tension coefficient for the liquid-gas interface, and $\kappa_j$ is the interface normal curvature in the *j*-direction

The third term on the R.H.S. of Equation (2) represents the momentum source term due to film gravitational body forces in the direction of the film flow. Finally, the fourth source term on the R.H.S. of Equation (2), $S_\tau$, represents the balance of viscous shear forces on the film, including contributions from the interfacial shear stress driving the film, $\tau_i$, and the wall shear stress resisting fluid flow over the stationary outer chamber wall, $\tau_c$. The viscous source term, $S_\tau$ may be computed according to Equation (3)

$$S_\tau = \frac{\tau_i - \tau_c}{\rho_l}. \tag{3}$$

The film interface shear is estimated from a non-linear interaction with the core gas flow model as described in Section 2.2. In addition to shear and gravity forces, the surface tension and pressure gradients are included in order to extend the model to complex film phenomena such as pooling and shocks where these forces have previously been shown to play a crucial role in solution stability and accuracy [7]. A film profile function is assumed a-priori and used to evaluate the inertia integral in Equation (2). In the present study, a quartic film velocity profile has been used, which is capable of adequately representing both planar unidirectional film flows as well as non-unidirectional films with local flow separation and re-circulations within the film.

For simplicity, the present film model ignores the effects of film momentum and core gas speed of the air entrained into the film and oil droplets suspended in the core flow. These conditions have however been observed to occur in bearing chamber representative conditions (See for instance the work of Budi et al [2]). Incorporating these effects is recommended as an area for future research and we envisage that this would involve the addition of a film scalar transport equation for the entrained air, with appropriate source and sink terms from the entrained air mass. This would be coupled to the film momentum equation (2) through an additional source terms to account for the effects of locally entrained air on the film velocity. A similar approach would be envisaged for the effect of suspended oil droplets on the core gas dynamics.

### 2.2. Core gas dynamics model

The core gas flow in the annular space of the chamber is set into motion by the momentum transfer from the rotating shaft. The rotating air also exchanges momentum with the incoming sealing air flow as well as the film coated stationary outer wall resulting in a mean core gas speed, $\bar{u}_g$.

A 1-D core gas dynamics model is used to estimate this core gas speed based on the principal of angular momentum conservation as previously described in [9] taking into account the effects of sealing air as well as the interface shear stress acting on the film. The azimuthal momentum balance is then given by Equation (4).

$$M_{shaft} - M_{film} = -M_{sealingAir}, \tag{4}$$

where $M_{shaft}$ is the shaft moment, $M_{film}$is the film interface moment and $M_{sealingAir}$is the momentum change associated with the incoming sealing air flow. The film interface is treated as a moving wall translating at the interface film speed, $u_i(s,t)$ and a smooth pipe analogy is used to idealise the core gas flow. The various moments due to the shaft and film effects on the core air flow may be estimated according to the following relations;

$$M_{shaft} = \tau_s A_s r_s = \tau_s (2\pi {r_s}^2 L), \tag{5}$$

$$M_{film} = \tau_i A_i r_i = \tau_i \big(2\pi (r_c - \bar{h})^2 L\big), \tag{6}$$

where $\tau_s$ is the shear stress on the rotating shaft, $\tau_i$ is the interfacial shear stress on the moving film, $r_c$ is the stationary chamber wall radius; $r_s$ is the rotating shaft radius; $\bar{h}$ is the mean film thickness along the chamber wall obtained from the film hydrodynamics model described in Section 2 and $L$ is the axial length of the chamber. Taking the smooth pipe analogy as in [9] the Blasius friction factor, $\lambda$, may be used to estimate the shaft and interface shear stresses according to;

$$\tau_s = \frac{\lambda_s}{8}\rho_g \big(\omega_s r_s - \bar{u}_g\big)^2, \tag{7}$$

$$\tau_i = \frac{\lambda_i}{8}\rho_g \big(\bar{u}_g - u_i\big)^2, \tag{8}$$

where $\rho_g$ is the gas density, $\omega_s$ is the shaft rotational speed, $\bar{u}_g$ is the mean azimuthal speed of the core gas and $u_i$ is the film interface speed which in the present study is obtained from the instantaneous mean film speed, $u_l(s,t)$, according to Equation (9). The

$$u_i(s,t) = \frac{3}{2}u_l(s,t). \quad (9)$$

The Blasius friction factors, $\lambda_s$ and $\lambda_i$ for the rotating shaft and the moving film interface are computed based on a smooth pipe analogy of the core air flow according to Equation (10) after [10].

$$\lambda_s = 0.316(Re_{g,s})^{-0.25} = 0.316\left(\frac{\rho_g D_h\left(\left|\omega_s r_s - \bar{u}_g\right|\right)}{\mu_g}\right)^{-0.25} \quad (10)$$

$$\lambda_i = 0.316(Re_{g,i})^{-0.25} = 0.316\left(\frac{\rho_g D_h\left(\left|u_i - \bar{u}_g\right|\right)}{\mu_g}\right)^{-0.25} \quad (11)$$

Where the hydraulic diameter of the core gas in the presence of the film is estimated as;

$$D_h = \left[\frac{4A}{U}\right] = \left[\frac{2L(r_c - \bar{h} - r_s)}{(L + r_c - \bar{h} - r_s)}\right], \quad (12)$$

Finally, the contribution from the sealing air flow is computed according to Equation (13).

$$M_{sealingAir} = \dot{m}_{g,in} r_{g,in}\left(u_{g,t,in} - \bar{u}_g\right) \quad (13)$$

By solving the governing momentum equation for the core gas flow, Equation (4), the mean core gas speed, $\bar{u}_g$, may be reliably estimated. The core gas flow model is coupled to the film hydrodynamics model through the interface film speed, $u_i$, which is obtained from the film hydrodynamics model used in (9) and (13) to estimate $\bar{u}_g$, and in turn, the interface shear stress, $\tau_i$ from the core gas model in (8) is used to drive the moving film. This results in a non-linear coupling between the two models. The core gas equation (4) was iteratively solved using the non-linear system solver fsolve in MATLAB.

## 3. Oil film thickness predictions and validation

### 3.1. Simulation cases

A set of simulations have been run and the results for film thickness and driving shear stress compared with the BCI bearing chamber cases reported by Gorse et al [9]. The BCI chamber consists of a rotating inner shaft of radius $r_s$= 64 mm (for the bare shaft), surrounded by a cylindrical chamber of annular height $(r_c - r_s) = 10$ mm and axial width $L = 15$ mm which correspond to the experimental setup of Gorse et al [9]. For all cases considered in this paper, a sealing air flow of $\dot{m}_{g,in} = 10$ g/s and oil feed flow rate of 100 l/h were applied. The sealing air inflow temperature and pressure were 373 K and 2.5 bar and the oil inlet temperature was also set to 373 K which are consistent with [9]. In order to account for the variability in oil temperature from inlet to the film, and the effects this has on oil viscosity, the same cases have been run at higher oil temperature of 423 K which is the maximum oil inlet temperature from the experimental setup of [9]. Table 1 shows the oil and air properties used in the simulations.

Table 1: Fluid properties

| Fluid | $\rho$ [kg/m$^3$] | μ [Pa.s] | $\sigma$ [N/m] |
|---|---|---|---|
| Air | 2.335 | 2.21e-5 | |
| Oil (423K) | 906 | 2.19e-3 | 0.025 |
| Oil (373K) | 939 | 4.65e-3 | |

The air properties were estimated using the ideal gas law at sealing air inlet conditions (T = 373 K and $p$ = 2.5 bar). The oil properties used are representative of a typical aero-engine oil at the air inlet temperatures of 373 K or an elevated maximum working temperature of 423 K.

Simulations were setup to cover the broad range of rotational shaft speeds, $4000 \text{ RPM} < \omega_s < 16000 \text{ RPM}$, similar to those explored in [9]. All cases were run at a scavenge ratio of 3 which is representative of typical test conditions such as in [2], and a sensitivity tests showed results to be fairly independent of variations in the scavenge ratio for higher scavenge ratios of up to 5.

Although some of the dimensions and operating conditions specified above are not engine representative, the main aim was to establish a benchmark of the model against the available experimental data in [9]. The model may then be applied to a range of specified operating conditions that are more engine representative.

### 3.2. Results and discussion

For each of the cases, the predicted film interface shear stress profile, wall shear stress profile, mean film thickness and mean flux were obtained from the coupled 1D gas-film dynamics model presented in this paper.

Figure 3 shows the interface shear stress distribution acting on the oil film for the 373 K cases with air only and droplet to film momentum transfer ignored. The model predicts an increase in shear stress with rising shaft speed similar to the findings of the semi-empirical core-gas models such as [9]. Increase in the shaft speed leads to a higher core gas speed due to increased momentum transfer from the rotating shaft to the core gas and consequently a higher interface shear stress on the film. The present coupled model appears to significantly under-predict the interface shear stress compared to previous models [9]. A possible explanation for this discrepancy is the absence of the equivalent interface shear due to droplet-film momentum transfer, which was initially ignored for the cases shown in Figure 3 by assuming that the incoming oil mass had the same

azimuthal velocity as the wall film. This assumption is however incorrect and is shown to give very low interface shear stress values and lead to an inaccurate film hydrodynamics solution. Although previous such as [9] did not explicitly account for the droplet momentum transfer to the film in the mathematical formulation, due to their semi-empirical nature – where oil film speed profile measurements at a specified location were used to estimate an interface shear stress – the droplet-film momentum transfer effect was implicitly included in the final shear stress along with the core gas shear contribution. In contrast, since in the present model, no a-priori data is used, the cases where droplet to film momentum transfer is neglected are expected to result in a lower reduced interface shear stress as the effective shear stress due to droplet to film momentum transfer is neglected.

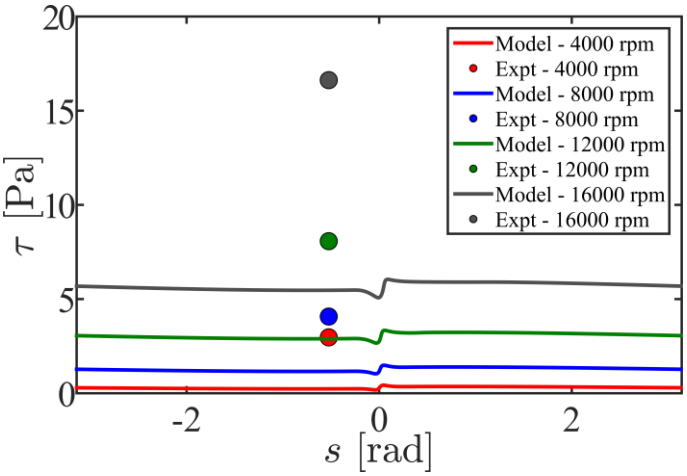


Figure 3: Coupled core gas-film model predictions for the wall shear stress distribution together with equivalent experimental measurements from Gorse [9]

To assess the impact of droplet-film momentum transfer on the shear stress and the resulting film dynamics, a set of cases were run which included an equivalent interface shear stress due to droplet impact. Oil droplet were assumed to impact the oil film with an azimuthal impact speed ranging from 0% - 50% of the mean core gas azimuthal speed. An equivalent droplet to film interface shear stress contribution is then included as a droplet interface shear as;

$$\tau_{i,d} = \dot{m}_d\left(k_d \bar{u}_g - u_i\right), \tag{14}$$

where $\tau_{i,d}$ is the interfacial shear stress due to droplet impact onto the film; $k_d$ is the droplet impact speed factor, with values ranging from 0% to 50%; $\dot{m}_d$ is the oil mass flow rate per unit surface area of the chamber wall which is obtained by uniformly distributing the oil feed flow. The model may however be configured to investigate the effect of spatial variabilities in the oil feed to the film.

The resulting interface shear stress distributions for a range of $k_d$ values (20%, 25% and 50%) are shown in Figure 4 together with results from cases run at 423 K and 373 K without any droplet contribution to momentum (i.e. $\tau_{i,d} = 0$ ). The effects of temperature variation on film interface shear stress are evaluated for temperatures of 373 K and 423 K in the case with no droplet momentum transfer and shown to be negligible for the range of speeds explored. Results with droplet impact effects included – where droplet impact speed, $u_d$ is not equal to the mean film speed, $\bar{u}_l$ – give improved agreement with the shear stress predictions from the semi-empirical model of Gorse [9] at the 330° location. Including droplet momentum is also shown to lead to a more spatially varying interface shear stress that is dependent on the local interface film speed, whereas this shear stress was previously assumed to be uniform. There is also a significant increase in the interface shear stress, with droplet impact included, and better agreement with the results from the semi-empirical Gorse model [9]. Of the speed ratios evaluated, the 25% ratio gave the best agreement in shear stress for the 4000 rpm case while the 20% ratio gave the best agreement for the rest of the cases. Further research and characterisation of the droplet to film momentum interaction is required in order to further calibrate the model and improve the overall shear stress prediction.

The corresponding film thickness profiles for each of the cases (shown in Figure 4 ) are also presented in Figure 5. The present model formulation is shown to be robust at predicting film thicknesses, remaining numerically stable throughout the chamber across the range of low shaft speeds (< 12000 rpm) where the Gorse model [9] was previously shown to breaks down. Including droplet momentum for higher shaft speed cases (c) and (d) was shown to lead to a smooth film regime, consistent with the experimental measurements, whereas the purely air shear cases incorrectly predicted a pooling solution near the sump due to interface shear under-estimation. This highlights the importance of droplet-film momentum transfer in accurate shear stress and film thickness predictions. For all cases, results for the droplet impact cases with azimuthal droplet impact speed ($u_d$) of 20 - 25% core gas speed ($u_g$) gave comparable predictions although there was significant disagreement with the experimental measurements from Gorse [9], particularly at the lower shaft speeds of less than 12000 rpm. Relatively better agreement was obtained at higher shaft speeds, although it should be noted that for instance at 16000 rpm, while the 25% ratio gave better agreement in the $-\pi < s < 0$ region, the 20% ratio performed better in the $0 < s < \pi$ region. This suggests a possible spatial variability in the azimuthal core-gas and droplet impact speeds across the chamber as well as a possible variation in droplet speed ratio with the shaft speed. Further work is required to explore these effects through an improved characterisation of droplet dynamics in a bearing chamber and improve the numerical accuracy of the film thickness predictions.

It should also be noted that for the 4000 rpm case, even with droplet impact, wall shear stress reversal was observed due to film backflow towards the sump (see Figure 4 (a)). This is further illustrated by the mean film speed and wall shear stress distributions for the 4000 rpm case and the 16000 rpm case (for comparison) shown in Figure 6. The localised peaks in wall

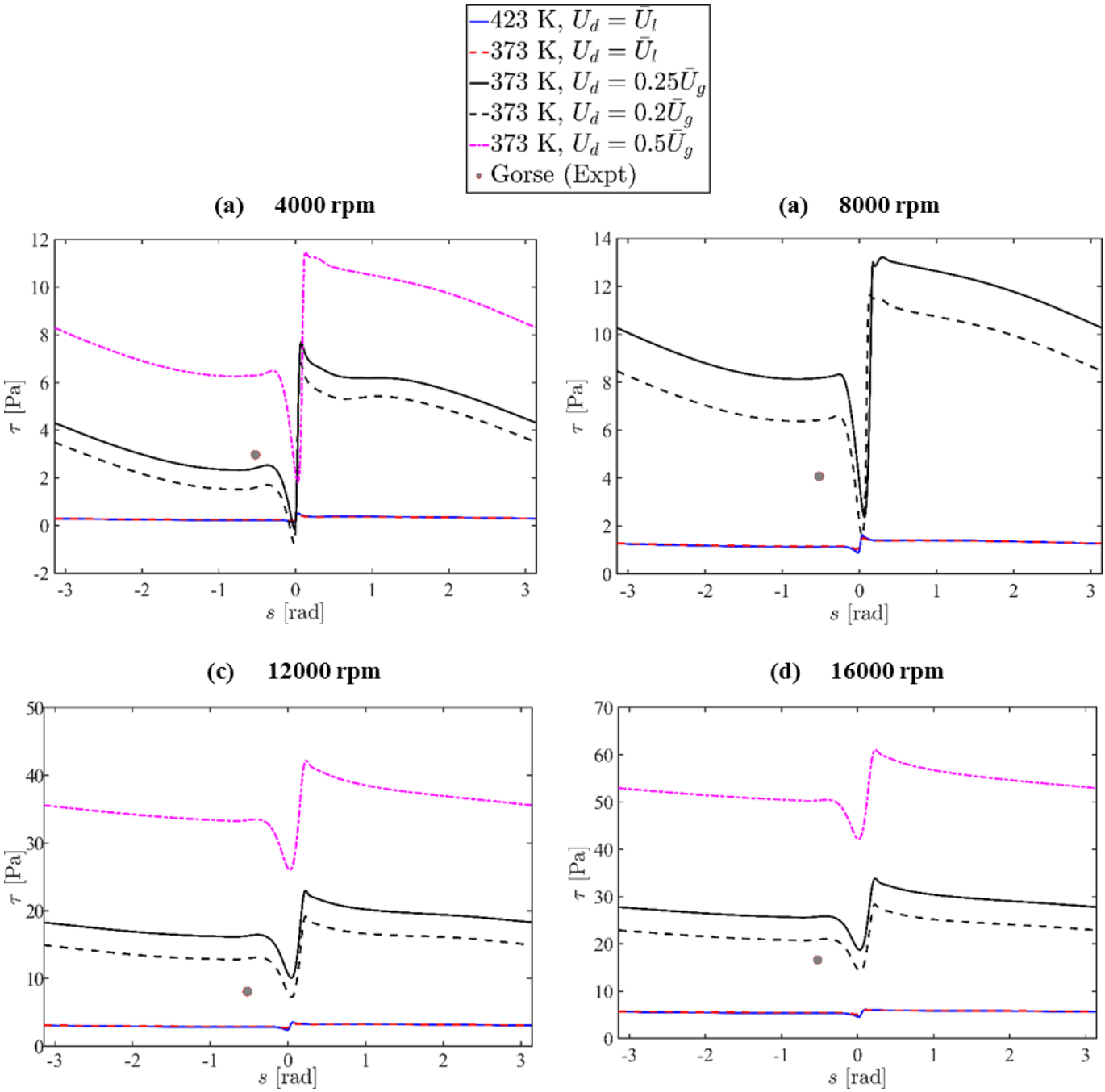


Figure 4: Predicted spatially variations in interface shear stress distributions from the present coupled gas-film model with and without droplet-film momentum transfer at rotational speeds of (a) 4000 rpm, (b) 8000 rpm, (c) 12000 rpm, (d) 16000 rpm. Also shown are the effects of film temperature and equivalent shear stress predictions at the 330° from the semi-empirical model of Gorse [9].

shear stress and film speed in the sump region are due to the near zero (dry film) conditions (see Figure 5 for thickness plots) which creates a mathematical singularity when subjected to the uniformly distributed droplet impact or air shear. These values may be ignored or filtered out of the analysis. For the 16000 rpm case, due to the high combined droplet and air interface shear of approximately 20 Pa (see Figure 4) the film is driven in a positive-s direction and a negative wall shear stress is observed throughout the domain, except at the sump discontinuity. The model however predicts a negative wall shear stress for the 4000 rpm case only in the s<0 region where gravity support film motion and in the s>0 region where gravity opposes the weal interface shear (approximately 4 Pa), a positive shear stress associated with the film successfully predicted to be flowing backwards towards the sump as shown in Figure 6(b). The induced interface shear stress is insufficient to circulate the film

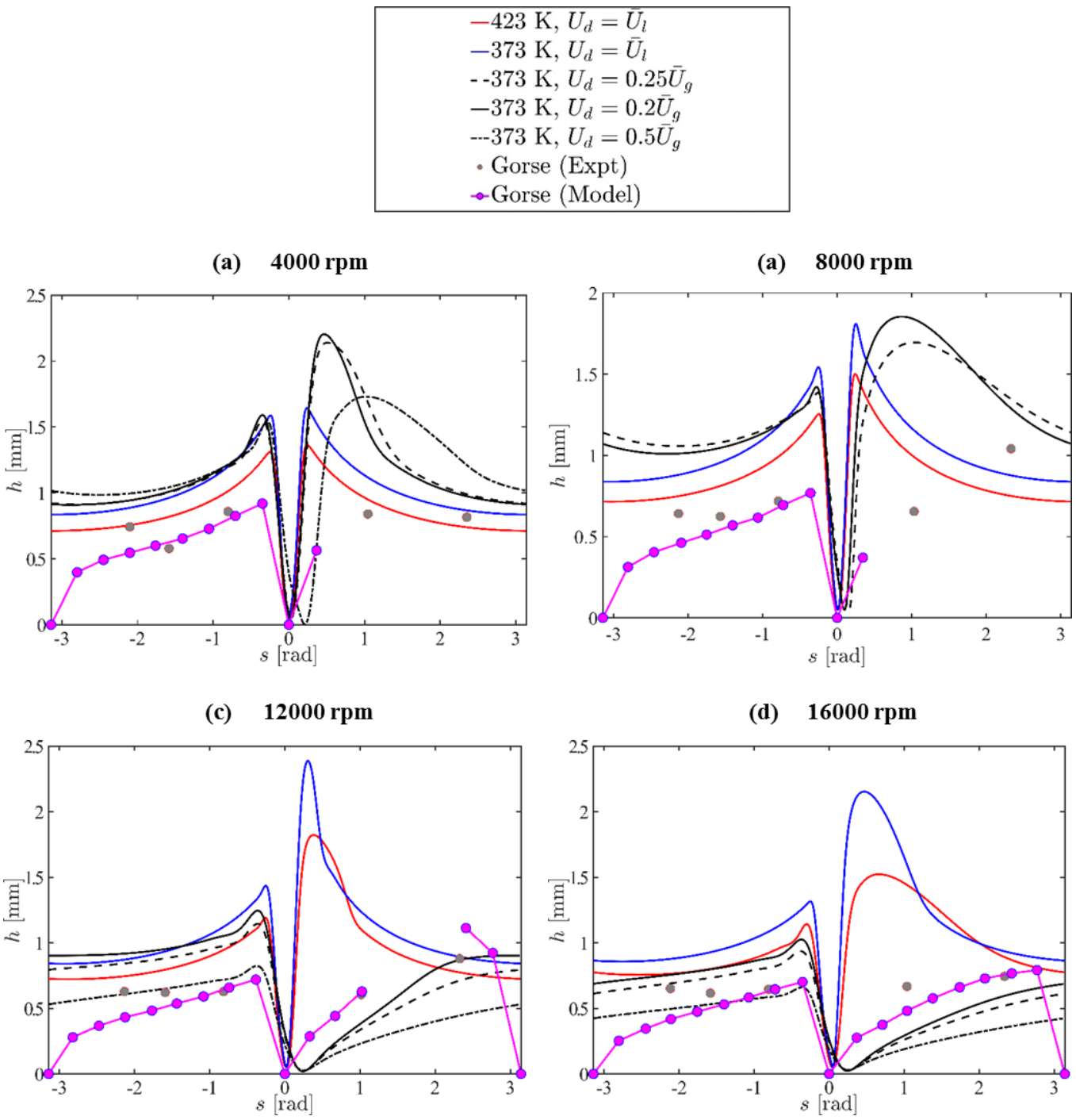


Figure 5: Predicted wall film thickness distributions from the present coupled gas-film model and the semi-empirical model of Gorse [9], showing the effects of droplet-film momentum transfer and film temperature at rotational speeds of (a) 4000 rpm, (b) 8000 rpm, (c) 12000 rpm, (d) 16000 rpm.

round the chamber to create a uni-directional film and a draining bi-directional film is formed. This behaviour is in agreement with observations by Gorse [9] in their experiments for the low shaft speed cases. The ability of the present model to predict this behaviour and accurately represents both film flow regimes is an improvement in model robustness over previous models such as [9] which were only stable at the high shaft speeds. As shown in the film thickness profiles in Figure 5, at lower shaft speeds where film backflow is expected a solution was not attainable in the s>0 portion of the domain for the Gorse model [9]. In these low shaft speed cases, the interface shear stress is relatively weak and unable to sustain a unidirectional film flow against gravitational forces.

In addition to the droplet effects, the model was used to explore sensitivity of results to oil film temperature. There is some uncertainty due to the discrepancy between inlet oil temperatures and the actual mean oil temperature in the liquid film which is expected to be higher after the oil has carried out its lubrication and cooling functions. The sensitivity of the film interface shear stress to temperature is however shown to be fairly minimal with both the 423 K and 373 K cases predicting fairly similar interface shear stress distributions across the range of shaft speeds as illustrated in Figure 4. Although the interface shear stress in these cases remained similar, the film profiles in Figure 5 showed that for all shaft speeds, an increase in film temperature is expected to lead to lower residence volume. This effect is largely due to the reduced viscosity of the film leading to faster flowing films in which injected oil is rapidly circulated and removed leaving a lower resident volume build-up.

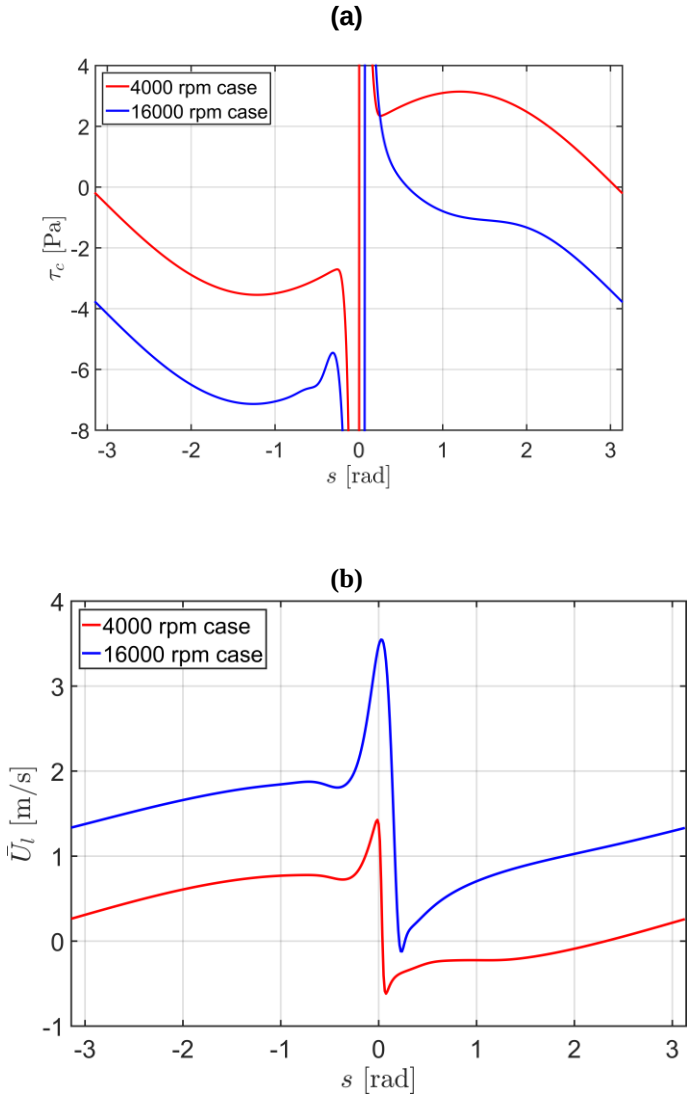


Figure 6: A comparison of; (a) wall shear stress distribution; and (b) mean film speed distribution; along the film wall for the 4000 rpm and 16000 rpm cases.

## 4. Conclusions

A model has been presented for the prediction of film thickness and velocity profiles of the shear driven liquid films inside an aero-engine bearing chamber rig under a range of conditions. The model presents a low cost approach for the rapid parametric evaluation of chamber designs during the preliminary stages of design with solutions obtainable in minutes as opposed to days of simulation as with conventional CFD models. This is largely due to the computationally efficient and numerically robust depth-averaged film hydrodynamics formulation which takes into account film inertia, pressure gradient and surface tension forces. These improvements are shown to guarantee that the model is able to resolve the key flow physics associated with regions where film backflow and re-circulations are expected at lower shaft speeds. Unlike previous models that are confined to applications with high shaft speeds, the present is robust and remains stable across the entire range of shaft speeds explored. A core gas model was successfully coupled to the film hydrodynamics model and used to model the non-linear gas-film momentum exchange and obtain a prediction for the core gas speed and interface shear stress. This non-linear coupling represents an additional improvement to existing bearing chamber analytical modelling. The model has been evaluated against existing experimental measurements from literature for oil film thickness in a test chamber. The air only shear stress model is shown to slightly over-predict film thicknesses and under-predict the interface shear stress, however including droplet-film momentum transfer through an equivalent droplet induced interface shear stress model is shown to lead to improved agreement with the experimental measurements. Further research is recommended in order to improve the robustness of this droplet-film momentum transfer model and include the effects of entrained air and suspended oil on air film and core gas dynamics. Oil film temperature was also shown to have a significant effect on oil film thickness distribution within the chamber due its impact on the film viscosity, although the impact on interface shear stress remained negligible.


## Acknowledgement

The research leading to these results has received funding from Rolls-Royce plc.


## Nomenclature

**Capital letters**

| | |
|---|---|
| $A$ | Area [m$^2$] |
| $L$ | Domain axial length [m] |
| $M$ | Moment [Nm] |
| $S$ | Depth-averaged source-term [m$^2$/s$^2$] |

**Lowercase letters**

| | |
|---|---|
| $h$ | Film thickness [m] |
| $\dot{m}$ | Mass flow rate [kg/s] |
| $p$ | Film pressure [Pa] |
| $q$ | Film flux [m$^2$/s] |
| $r$ | Radius of curved surface [m] |
| $s$ | Azimuthal coordinate [m] |
| $u$ | Tangential speed [m/s] |
| $\bar{u}$ | Mean tangential speed [m/s] |

**Greek symbols**

| | |
|---|---|
| $\kappa$ | Interface curvature [1/m] |
| $\lambda$ | Blasius friction factor [] |
| $\mu$ | Dynamic viscosity [Pa.s] |
| $\rho$ | Density of air [kg/m$^3$] |
| $\sigma$ | Surface Tension Coefficient [N/m] |
| $\tau$ | Shear stress [Pa] |

**Subscripts**

| | |
|---|---|
| *c* | Stationary outer chamber wall |
| *d* | Droplet |
| *g* | Core gas |
| *g,in* | Sealing air inlet |
| *h* | Hydraulic |
| *i* | Air-Oil interface |
| *l* | Liquid film |
| *s* | Rotating inner shaft (not to be confused with the azimuthal *s* coordinate) |
| *y* | Wall-normal direction |

## 5. References


[1] Kurz W. and Bauer H.-J., 2014, "An Approach for Predicting the Flow Regime in an Aero Engine Bearing Chamber," in *ASME Turbo Expo 2014: Turbine Technical Conference and Exposition*, Dusseldorf

[2] Chandra B. and Simmons K. A., 2014, "Transient Two-Phase Effects in an Aeroengine Bearing Chamber Scavenge Test Rig," in *ASME 2014 International Mechanical Engineering Congress and Exposition, Volume 1: Advances in Aerospace Technology*, Montreal

[3] Glahn A. and Wittig S., 1996, "Two-phase air/oil flow in aeroengine bearing chambers: charaterisation of oil film flow," *J. Eng. Gas Turbines Power,* vol. 118, no. 3, pp. 578-583

[4] Adeniyi A. A., Morvan H. P. and Simmons K. A., 2014, "A Transient CFD Simulation of the Flow in a Test Rig of an Aeroengine Bearing Chamber," in *ASME Turbo Expo 2014: Turbine Technical Conference and Exposition*, Dusseldorf

[5] Bristot A., Morvan H. P. and Simmons K. A., 2016, "Evaluation of a Volume of Fluid CFD Methodology for the Oil Film Thickness Estimation in an Aero-Engine Bearing Chamber," in *ASME Turbo Expo 2016: Turbomachinery Technical Conference and Exposition*, Seoul

[6] Farrall M., Simmons K. A., Hibberd S. and Gorse P., 2004, "A Numerical Model for Oil Film Flow in an Aeroengine Bearing Chamber and Comparison to Experimental Data," *J. Eng. Gas Turbines Power,* vol. 128, no. 1, pp. 111-117

[7] Kakimpa B., Morvan H. P. and Hibberd S., 2016, "The Depth-Averaged Numerical Simulation of Laminar Thin-Film Flows With Capillary Waves," *J. Eng. Gas Turbines Power,* vol. 138, no. 11, pp. Paper No: GTP-16-1105

[8] Kay E. D., Hibberd S. and Power H., 2014, "A depth-averaged model for non-isothermal thin-film rimming flow," *Int. J. Heat Mass Tran.,* vol. 70, p. 1003–1015

[9] Gorse P., Busam S. and Dullenkopf K., 2006, "Influence of operating condition and geometry on the oil film thickness in aeroengine bearing chambers," *J. Eng. Gas Turbines Power,* vol. 128, pp. 103-110

[10] Blasius P. R. H., 1913, "Das Aehnlichkeitsgesetz bei Reibungsvorgangen in Flussigkeiten," *Forschungsarbeiten auf dem Gebiete des Ingenieurwesens.*